Resolving strong-field tunneling ionization with a temporal double-slit interferometer

Jia Tan,[1] Yueming Zhou ●,[1,*] Qinghua Ke,[1] Mingrui He,[1] Jintai Liang,[1] Yang Li,[1] Min Li,[1] and Peixiang Lu[1,2,†]

[1]*School of Physics and Wuhan National Laboratory for Optoelectronics,*
Huazhong University of Science and Technology, Wuhan 430074, China

[2]*Hubei Key Laboratory of Optical Information and Pattern Recognition, Wuhan Institute of Technology, Wuhan 430205, China*

Laser-induced tunneling ionization is one of the most fundamental and ubiquitous quantum processes and it initiates various ultrafast phenomena in intense laser-atom and laser-molecule interactions. Accurately resolving tunneling ionization is essential for understanding these phenomena. Based on the advanced attosecond technologies, such as high-order harmonic spectroscopy and strong-field photoelectron holography, previous studies have resolved the temporal properties of the tunneling process for rescattering electron. Here, as a complement, we theoretically demonstrate the retrieval of the time information of the tunneling process for the direct electron with the temporal double-slit interferometer. In this scheme, a weak second harmonic parallel to the fundamental field is added. By solving the time-dependent Schrödinger equation, the photoelectron momentum distribution (PEMD) from strong-field tunneling ionization is obtained. Varying the relative phase of the parallel two-color field, the path of the ionized electrons periodically changes, leading to a shift of the time double-slit interference fringes in PEMDs. By analyzing the response of the interference fringes to the perturbation, the time information of direct electron in strong-field tunneling ionization is reconstructed. Interestingly, our results present excellent agreement with the complex time obtained from the quantum-orbit model.

I. INTRODUCTION

Laser-induced tunneling ionization is the first step of a broad range of strong-field phenomena, such as above-threshold ionization (ATI) [1,2], high-order harmonic generation [3–6], and nonsequential double ionization [7–12], and it lies at the heart of attosecond science [13,14]. During past decades, the relationship between the tunneling of an electron through a barrier and its dynamics outside the barrier, and how to resolve the tunneling ionization process have been hotly discussed [15–18]. Recently, the advances in attosecond technology have opened a door to revisit this issue. For instance, with high-order harmonic spectroscopy, the ionization time for each harmonic has been reconstructed [19,20]. Very recently, with photoelectron spectroscopy, the temporal properties for the tunneling ionization process of photoelectrons have been accurately retrieved with the concept of photoelectron holography [21–23].

For the tunneling ionization of an atom or a molecule in a strong laser field, part of the ionized electron wave packet (EWP) would be driven back and scatter off with the ionic core (rescattering electron), while the other part of the EWPs reach the detector directly without further interaction with the patent ion (direct electron) [24]. In a quantum mechanism, the temporal properties of the direct and rescattering EWPs have been conceptually defined with the quantum orbit (QO) model, which is based on the application of the Feynman's path-integral approach in describing strong-field laser-atom interaction [25]. In the above-mentioned high-order harmonic spectroscopy and photoelectron spectroscopy, the temporal properties for the rescattering electron were retrieved, and the results were in good agreement with the predictions of the QO model [19–22]. According to the QO model, the temporal properties of the direct electron are actually very different from that of the rescattering electrons [25]. In strong-field tunneling ionization, the probability of the rescattering electron is small and it contributes significantly to the high-energy part of the photoelectron spectrum [2]. The direct electron plays a major role in the photoelectron momentum distribution (PEMD). However, the temporal properties for this direct electron have not been measured yet. We should mention that in the attoclock experiment, the temporal properties of the tunneling process for the direct electron have been deeply investigated [26–28]. In those measurements, the time was defined as the real-time delay between the laser electric-field peak and the ionization-rate peak. Quantum mechanical, tunneling ionization occurs continuously and the electron with different final momenta is tunneling ionized at different times. In the QO model, ionization time is a complex number. The real part denotes the time when an electron exits a tunneling barrier, and the imaginary part characterizes the underbarrier electron motion [29,30]. Here, by surveying the interference structures in the PEMDs, we study this complex ionization time of the direct election.

Due to the coherent nature of tunneling, the tunneled EWPs following different pathways to the same final momentum will give rise to numerous interesting interference patterns in PEMDs. In the past ten years, these interference structures

*zhouymhust@hust.edu.cn
†lupeixiang@hust.edu.cn
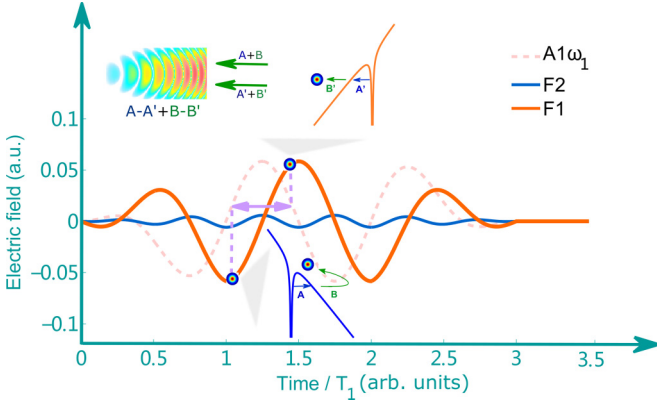
FIG. 1. The schematic diagram of the temporal double-slit interferometer. The red and blue curves show the FM field $\vec{F}_1$ and SH component $\vec{F}_2$ of the parallel two-color field, respectively. The peak intensity ratio of the two components is 100/1 (i.e., $F_1/F_2 = 10/1$). The dashed red curve denotes the vector potential $\vec{A}_1$ of the FM field and is scaled by its frequency ω_1. Strong-field tunneling ionization of atoms and molecules produces EWPs at the rising edge (the top inset) and descending edge (the bottom inset) of the electric field interfere in the PEMD, giving rise to the temporal double-slit interference. This interference is determined by the phase differences of the EWPs accumulated during their propagation under the tunneling barrier $(A - A')$ and in the continuum $(B - B')$. When a weak perturbation is added, the phase differences change, and thus the interference structure shifts. Analyzing the response of the interference structure to the weak perturbation, the temporal properties for this double-slit interferometer are determined.

have been identified and comprehensively studied. The well-known strong-field photoelectron holographic interference is one of them [31,32]. Here, we employ another interference, i.e., the temporal double-slit interference [33,34]. This structure derives from the interference of two direct EWPs released within the consecutive laser half cycles at times where the vector potential is the same but the direction of electric field is opposite. It leads to the modulation of ATI spectrum, offering abundant information on the subcycle dynamics [35–37]. In Ref. [33], the temporal double-slit interference was first observed in experiments for argon, and subsequently it has been experimentally and theoretically analyzed [38–40]. Recently, a two-color pulse was used to control the temporal double-slit interference and to extract the phase difference of the two direct EWPs after tunneling [41–44]. In this paper, we use this temporal double-slit interferometer to accurately determine the complex ionization time of the direct electron.

The schematic diagram of our scheme is illustrated in Fig. 1, where we add a weak perturbative second harmonic (SH) to the strong fundamental (FM) field. The perturbation affects the phases of the two paths of EWPs in the temporal double-slit interferometer, and thus leads to the shift of the interference in the PEMDs. As the relative phase of this two-color field changes, the interference fringes oscillate accordingly. By analyzing the response of the interference fringes to the perturbation, the temporal properties for the EWPs could be retrieved. It should be noted that in the temporal double-slit interferometer, the effect of the long-range Coulomb potential on the phases of the EWPs is the most difficult issue in

previous studies [36,38,39]. In our scheme, we analyze the shift of the interference fringes induced by the weak perturbation, and we are free from the effect of the Coulomb potential. Our analysis shows that the amplitude of the oscillation of the interference fringes is very sensitive to the complex ionization time of tunneling. Based on this result, the imaginary part of the ionization time is accurately retrieved. The obtained results are in remarkable agreement with the predictions of the QO model.

II. THEORETICAL METHODS

A. Numerically solving TDSE

To investigate the temporal double-slit interference of PEMDs in parallel two-color laser pulse, we numerically solve the two-dimensional time-dependent Schrödinger equation (2D-TDSE) in the coordinate (x, y). Atomic units (a.u.) are used throughout unless stated otherwise. In the length gauge, the TDSE is given by

$$i\frac{\partial \Psi(\vec{r}, t)}{\partial t} = \left[-\frac{1}{2}\nabla^2 + V(r) + \vec{r} \cdot \vec{F}(t) \right]\Psi(\vec{r}, t), \quad (1)$$

where $\Psi(\vec{r}, t)$ represents the wave function and $\vec{r}$ denotes the electron position. $V(r) = -1/\sqrt{x^2 + y^2 + \eta}$ is soft-core potential and its soft-core parameter η is set to be 0.39 to match the ionization potential of argon ($I_p = 0.58$ a.u.). $\vec{F}$ represents the electric field of the laser pulse, which is combined by a strong FM field and a weak SH component, respectively. In our calculation, $\vec{F}$ is written as

$$\vec{F}(t) = f(t)[F_1 \cos(\omega_1 t) + F_2 \cos(\omega_2 t + \varphi)]\hat{x}, \quad (2)$$

where $\hat{x}$ denotes the polarization direction of the parallel two-color field and φ represents the relative phase. $f(t)$ is the envelope function of the laser pulse, which has the form of $f(t) = \sin^2(\pi t/T_p)$ with duration time $T_p = 8T_1$ ($T_1 = 2\pi/\omega_1$). ω_1 and ω_2 indicate the frequencies of the FM field and SH component, respectively.

To solve the 2D-TDSE, the initial wave function is prepared by the imaginary-time propagation [45]. The split-operator method is used on a Cartesian grid $\zeta \times \zeta$ with $\zeta = 500$ a.u [46]. The time step is fixed at $\Delta t = 0.1$ a.u. and the spatial discretization is $\Delta x = \Delta y = 0.24$ a.u. The whole wave function is smoothly divided into two regions: the inner region and the outer region by a splitting function [47]. In the inner space, the wave function Ψ_1 propagates under full Hamiltonian, while in the outer space, the wave function Ψ_2 standing for the "ionized part" analytically propagates under the Volkov Hamiltonian. More specifically, at each time step, Ψ_2 is firstly Fourier transformed into the momentum space $C(\vec{p}, \tau)$, and further it is propagated from time τ to the end of the laser pulser. Finally, the PEMD is obtained by summing the wave function $\overline{C}(\vec{p}, \tau) = e^{-i\int_\tau^\infty \frac{1}{2}[\vec{p}+\vec{A}(\tau')]^2 d\tau'} C(\vec{p}, \tau)$ in the momentum space over τ,

$$\frac{dP(\vec{p})}{dEd\theta} = \sqrt{2E}\left| \sum_\tau \overline{C}(\vec{p}, \tau) \right|^2, \quad (3)$$

where $\vec{p}$ is the electron final momentum, $E = \vec{p}^2/2$ is the electron energy, $\vec{A}(\tau) = -\int_{-\infty}^\tau \vec{F}(t)dt$ is the laser vector potential, and θ denotes the electron emission angle. At the end

of the laser pulse, the wave function is propagated for four additional optical cycles of the laser pulse to make sure that the "slow" electrons exceed the boundary of the inner space [48,49].

B. Quantum-orbit model

To analyze the photoelectron interferometer, the strong-field approximation (SFA) method is employed [50,51]. In this method, the strong-field ionization process is described by the transition amplitude from the initial ground state ψ_0 with binding energy of $-I_p$ to the final continuum state $\psi_{\vec{p}}$. For the direct electron, the transition matrix element is expressed as

$$M_{\vec{p}}^D = -i \int_0^{t_f} dt \langle \vec{p} + \vec{A}(t) | \vec{r} \cdot \vec{F}(t) | \psi_0 \rangle e^{[iS^D]}, \quad (4)$$

where t_0 is the ionization time, t_f is the pulse turn-off time, and

$$S^D = -\int_{t_0}^{t_f} \left\{ \frac{1}{2} [\vec{p} + \vec{A}(\tau)]^2 + I_p \right\} d\tau \quad (5)$$

is the electron action. In our study, the temporal double-slit interference of PEMD comes from the interference of two direct EWPs, and it is given by

$$|M_{\vec{p}}|^2 = \left| M_{\vec{p}}^{D_1} + M_{\vec{p}}^{D_2} \right|^2$$
$$= \left| M_{\vec{p}}^{D_1} \right|^2 + \left| M_{\vec{p}}^{D_2} \right|^2 + 2 \left| M_{\vec{p}}^{D_1} \right| \left| M_{\vec{p}}^{D_2} \right| \cos(\Delta\theta). \quad (6)$$

Here $M_{\vec{p}}^{D_1}$ and $M_{\vec{p}}^{D_2}$ denote the ionization amplitudes of the tunneling EWPs, and $\Delta\theta$ represents its phase difference. $M_{\vec{p}}^{D_1}$ and $M_{\vec{p}}^{D_2}$, indicating the two temporal slits, serve as the two arms of our interferometer. The interference structure is determined by the phase difference of the transition amplitude mainly. Thus, in the following, for simplicity we will omit the pre-exponential term of transition matrix.

According to Ref. [31], the phase difference for the temporal double-slit interference is obtained by the saddle-point approximation, which provides us the QOs to analyze the interference structure. In a single-color field, it is written as

$$\Delta\theta^S = S^{D_2} - S^{D_1}$$
$$= -\int_{t_0^{D_2}}^{t_f} \left\{ \frac{[\vec{p} + \vec{A}(\tau)]^2}{2} + I_p \right\} d\tau$$
$$+ \int_{t_0^{D_1}}^{t_f} \left\{ \frac{[\vec{p} + \vec{A}(\tau)]^2}{2} + I_p \right\} d\tau$$
$$= \int_{t_0^{D_1}}^{t_0^{D_2}} \left\{ \frac{[\vec{p} + \vec{A}(\tau)]^2}{2} + I_p \right\} d\tau, \quad (7)$$

where $t_0^{D_1}$ and $t_0^{D_2}$ denote the ionization times of the two direct EWPs. When a SH parallel to the single-color field is added, the phase difference is rewritten as

$$\Delta\theta^{\mathrm{PTC}} = \int_{t_0^{D_1}}^{t_0^{D_2}} \left\{ \frac{[p_x + \vec{A}_1(\tau) + \vec{A}_2(\tau)]^2 + p_y^2}{2} + I_p \right\} d\tau. \quad (8)$$

In our two-color scheme, the additional SH is much weaker than the FM field and is used to perturb the subsequent motion

of EWP. Therefore, the ionization time of the direct electron is not affected by the weak perturbation, and it is approximately determined by the saddle-point equation in the FM field, i.e.,

$$\frac{1}{2}\left[p_x + \vec{A}_1\left(t_0^{D_1}\right)\right]^2 + \frac{1}{2}p_y^2 + I_p = 0,$$
$$\frac{1}{2}\left[p_x + \vec{A}_1\left(t_0^{D_2}\right)\right]^2 + \frac{1}{2}p_y^2 + I_p = 0. \quad (9)$$

Here, Eqs. (9) have a transparent physical interpretation, representing the energy conservation of photoelectron at the moment of ionization.

It should be noted that the ionization times obtained from Eqs. (9) are complex numbers, so the phase differences in Eqs. (7) and (8) are complex. The imaginary part related to the amplitude of direct EWP affects the contrast of interference fringes, and the real part decides the position of fringes that we are interested in. Hence, in this paper we consider the real phase difference only.

III. RESULTS AND DISCUSSION

The TDSE results of PEMDs for strong-field tunneling ionization of an Ar atom are illustrated in Figs. 2(a)–2(d), where Fig. 2(a) shows the data of 1600-nm single-color laser field, and Figs. 2(b)–2(d) present the data of the parallel two-color pulse with relative phases $\varphi = 0$, 0.5π, and 1.5π, respectively. The parallel two-color field is polarized along x direction, and consists of a strong 1600-nm FM field and a much weaker SH. The laser peak intensity for the 1600-nm laser pulse is 1.2×10^{14} W/cm^2 and that for the SH component is 1.2×10^{12} W/cm^2. In these PEMDs, there are three types of interference fringes. The first one is the inter-cycle interference, and it is a ringlike structure in the PEMD and presents as the peak structure in the energy spectrum. This pattern stems from the interference of the EWPs created at a time interval separated by the laser cycle and is referred to as an ATI peak [52,53]. The second type of the interference exhibits the almost parallel fringes in the PEMD (parallel to the laser polarization direction), known as strong-field photo-electron holography [31]. It is originated from the coherent su-perposition of the direct and near-forward rescattering EWPs tunneled at the same quarter of the laser cycle. During the past years, this structure has been broadly studied and applied to probe the structural and temporal properties of atomic and molecular systems with angstrom and attosecond precision [54–62]. The third one, the most prominent at the high-energy region of the PEMDs in Figs. 2(a)–2(d), presents as the modulation of ATI rings. It results from the interference of the direct EWPs tunneled ionized during two adjacent half cycles of the laser pulse and is described as the temporal double-slit interference [33]. In recent studies, this subcycle interference has attracted much attention and has been shown that it could supply a wealth of information on the subcycle dynamics [35–37,63]. Here, we focus on this type of interference.

In Figs. 2(a)–2(d), it is seen that the temporal double-slit interference is strongly disturbed by the perturbative SH field. For example, with respect to the cut of $p_x = -1.3$ a.u. (the vertical dashed line), the temporal double-slit inference fringes in the two-color field are shifted along the p_x direction. This can be more clearly seen in Figs. 2(e) and 2(f), where we display two cuts of PEMD as functions of φ for $p_x \in$
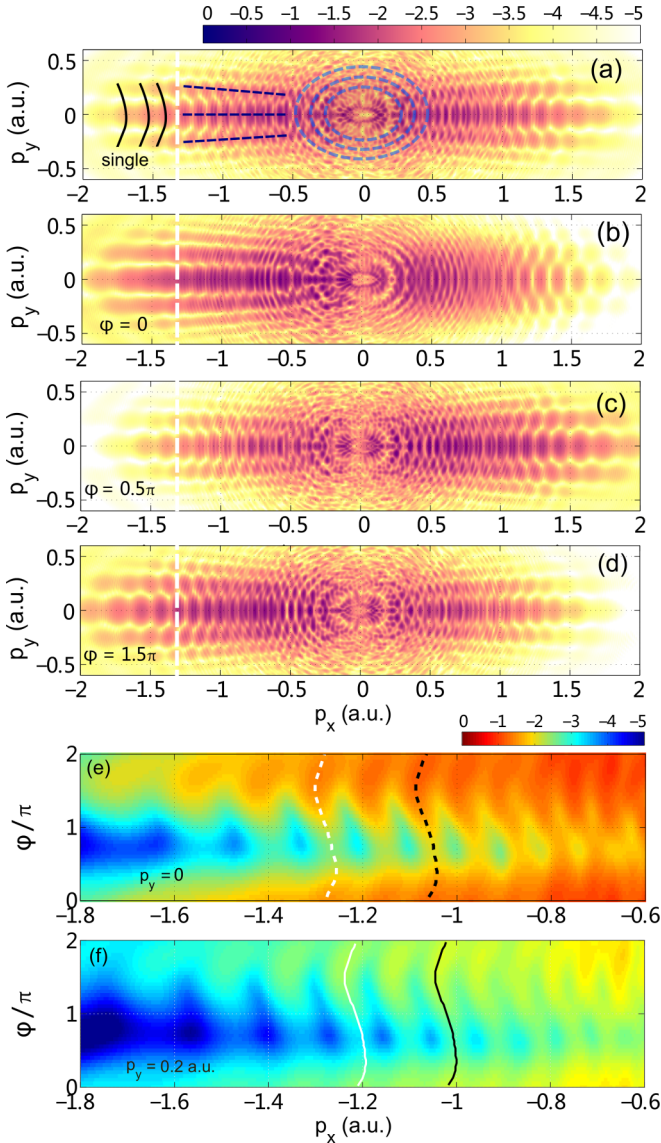
FIG. 2. (a)–(d) PEMDs of argon atom obtained by solving TDSE in the 1600-nm single-color field and parallel two-color fields with the relative phases $\varphi = 0$, 0.5π and 1.5π, respectively. The parallel two-color field is polarized along the x axis, and synthesized by a strong 1600-nm FM field and a weak SH. The dashed white lines indicate the cut of $p_x = -1.3$ a.u. The dashed circles, solid curves, and black dashed lines show the ATI peaks, temporal double-slit structure, and holographic structure, respectively. (e) Photoelectron yield at $p_y = 0$ for φ ranging from 0 to 2π. (f) Same as (e) but for another cut of $p_y = 0.2$ a.u. The dashed and solid curves show the position of the temporal double-slit interference maxima. All the color bars of PEMDs are logarithm scaled.

$[-1.8, -0.6]$ a.u. It is shown that for the cut of $p_y = 0$, the interference fringes periodically oscillate with the relative phase φ, and they shift most to the left side at $\varphi = 1.5\pi$, while to the right side at $\varphi = 0.5\pi$. For the cut of $p_y = 0.2$ a.u., the behavior is similar to that of $p_y = 0$. As we will demonstrate, this fringe shift allows us to resolve the time information on the direct electron in a strong-field tunneling ionization process.
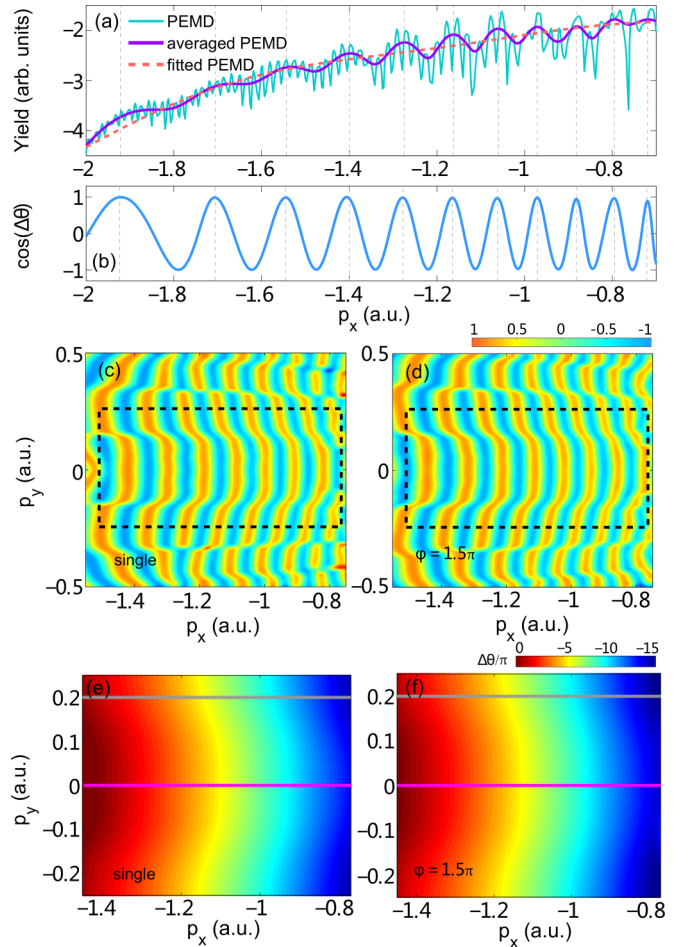
FIG. 3. (a) TDSE results of PEMD for single-color laser field at $p_y = 0$ before (solid green curve) and after (solid purple curve) averaging over the ATI peaks. The dashed red curve indicates the factor $e^{f(p_x)}$. (b) Interference term $\cos(\Delta\theta)$ extracted from the averaged PEMD at $p_y = 0$ (solid blue curve). The dashed gray lines denote the positions of the time double-slit interference maxima. (c), (d) $\cos(\Delta\theta)$ obtained from the PEMD in the single-color field and the parallel two-color laser field with $\varphi = 1.5\pi$, respectively. (e), (f) Phase difference $\Delta\theta$ extracted from the momentum region of the dashed black boxes in (c) and (d), respectively. The purple and gray lines show the cuts of $p_y = 0$ and $p_y = 0.2$ a.u.

To extract the interference term of the temporal double-slit interference, we apply the following procedure to the PEMDs. First, we eliminate the ATI peaks and holographic structure by averaging the PEMD with a momentum window, i.e., over (p_x, p_y) in an interval $(p_x \pm \Delta p_x, p_y \pm \Delta p_y)$ of suitable widths $2\Delta p_x$ and $2\Delta p_y$. A cut of the thus obtained averaged PEMD as well as the raw TDSE results are presented in Fig. 3(a). It is clearly shown that the temporal double-slit interference behaves as a modulation to the cut. Then, we fit the averaged cut with the function of $e^{f(p_x)}[1 + g(p_x)\cos(\Delta\theta)]$, where $e^{f(p_x)}$ is the background contribution and is obtained by fitting the logarithmic PEMD with a polynomial. $g(p_x)$ represents the envelop of the oscillating function $\cos(\Delta\theta)$ and is again obtained by fitting with a polynomial. An example of $e^{f(p_x)}$ at the cut of $p_y = 0$ marked by the dashed line is shown in Fig. 3(a). Dividing the averaged PEMD by the factors $e^{f(p_x)}$

and $g(p_x)$, the interference term $\cos(\Delta\theta)$ is constructed. It lies between -1 and $+1$, as shown in Fig. 3(b). We repeat the above procedures for p_y ranging from -0.5 a.u. to 0.5 a.u. The extracted interference term from the PEMD for the single-color field is shown in Fig. 3(c), and that for the two-color field with $\varphi = 1.5\pi$ is shown in Fig. 3(d). Note that $\cos(\Delta\theta)$ is stable and independent on the details of the fitting calculations for the momentum region not very close to the classical boundaries of the PEMDs.

To show the effect of the perturbative SH field on the temporal double-slit interference quantitatively, we further extract $\Delta\theta$ from the interference term $\cos(\Delta\theta)$. The results are presented in Figs. 3(e) and 3(f). Then, we calculate the difference of $\Delta\theta$ in the two-color field with respect that of the single-color field, i.e., $\delta\theta = \Delta\theta^{\mathrm{PTC}} - \Delta\theta^S$, where $\Delta\theta^{\mathrm{PTC}}$ and $\Delta\theta^S$ represent the phase differences of the temporal double-slit interference fringes in the parallel two-color field and single-color field, respectively. Two examples of $\delta\theta$ at the cuts of $p_y = 0$ and $p_y = 0.2$ a.u. for several relative phases are shown in Figs. 4(a) and 4(b), respectively. The effect of the SH field is obviously seen. For example, for the cut of $p_y = 0$, $\delta\theta > 0$ and it increases with increasing p_x at $\varphi = 0.5\pi$, while for $\varphi = 1.5\pi$, $\delta\theta < 0$ and it decreases with increasing p_x. In Figs. 4(c) and 4(d), tracing $\delta\theta$ as function of φ for different p_x, it is indicated that $\delta\theta$ oscillates with φ, and the oscillate amplitude depends on p_x. For instance, for the photoelectron with the final momentum $(-0.9, 0)$ a.u., the amplitude for the oscillation of $\delta\theta$ equals to 0.6π, and for $(-1.1, 0)$ a.u., it is 0.4π. The behavior of the cut at $p_y = 0.2$ a.u. is similar to that of $p_y = 0$.

As demonstrated in Sec. II, the temporal double-slit interference can be described by Eqs. (7) and (8) in the single-color and parallel two-color field. It should be mentioned that Eqs. (7) and (8) stem from the SFA [25]. In SFA, the phase produced by the Coulomb interaction between the parent ion and ionized electron is not taken into account. Thus, the predicted interference structures deviate seriously from the TDSE calculations and experimental data [36,38,39]. In our scheme, the effect of Coulomb potential on the interference fringes in the single-color field is similar to that in the parallel two-color field, and it does not contribute to the shift of the interference fringes. So, we are free from dealing with this tedious issue. The reason is explained in the following.

As demonstrated in Ref. [41], the temporal double-slit interference could be quantitatively described when the phase which accounts for the Coulomb interaction is added to Eqs. (7) and (8). Therefore, the phases for the temporal double-slit interference in the single-color and two-color fields are rewritten as $\Delta\theta^{\mathrm{PTC}} + \alpha^{\mathrm{PTC}}$ and $\Delta\theta^S + \alpha^S$, respectively. The phase $\delta\theta$ responsible for the interference shift of the two-color field with respect to that of the single-color field is written as $\delta\theta = \Delta\theta^{\mathrm{PTC}} + \alpha^{\mathrm{PTC}} - \Delta\theta^S - \alpha^S$, where α^{PTC} and α^S represent the phases of the direct EWPs induced by the Coulomb interaction in the parallel two-color field and single-color field, respectively. The calculation about α is extraordinarily complicated in general. However, in our two-color field, the SH field is a perturbation, and the phase for the two-color laser field is approximately equaling to that of the single-color field, i.e., $\alpha^{\mathrm{PTC}} \doteq \alpha^S$. Thus, $\delta\theta$ could be
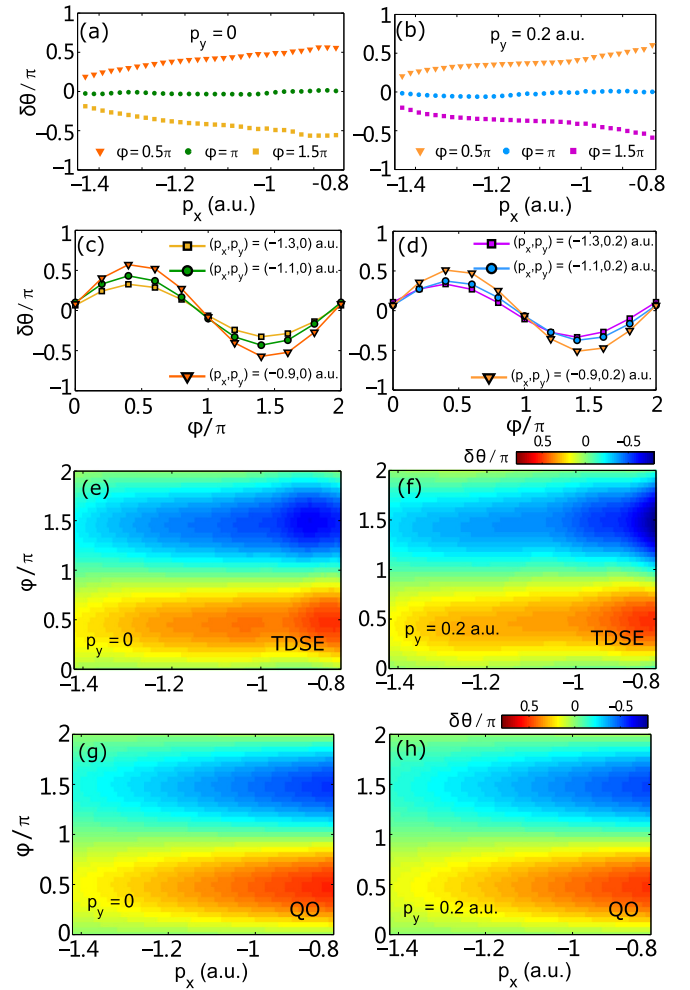
FIG. 4. (a) $\delta\theta$ at the cut of $p_y = 0$ for relative phase $\varphi = 0.5\pi$ (triangles), π (dots), and 1.5π (squares). (c) $\delta\theta$ as a function of φ for the photoelectron with the final momentum $(p_x, p_y) = (-0.9, 0)$ a.u. (triangles), $(-1.1, 0)$ a.u. (dots), and $(-1.3, 0)$ a.u. (squares). (e) $\delta\theta$ extracted from the averaged PEMDs at the cut of $p_y = 0$ for $\varphi \in [0, 2\pi]$ and $p_x \in [-1.4, -0.8]$ a.u. (g) $\delta\theta$ calculated by the QO model as a function of φ at the cut of $p_y = 0$ for $p_x \in [-1.4, -0.8]$ a.u.. (b), (d), (f), and (h) are the same as (a), (c), (e), and (g) but for the cut of $p_y = 0.2$ a.u.

written as

$$\delta\theta = \Delta\theta^{\mathrm{PTC}} - \Delta\theta^S. \tag{10}$$

This indicates that the Coulomb interaction does not affect the shift of the interference fringes, though it influences the positions of the interference fringes. Thus, it can be canceled out safely. This point is further confirmed by the good agreement between the predictions from Eq. (10) [Figs. 4(g) and 4(h)] and the TDSE results [Figs. 4(e) and 4(f)].

For our parallel two-color field, the SH field is a weak perturbation, and thus it is a good approximation that $\mathrm{Im}[t_0^{D_1}] = \mathrm{Im}[t_0^{D_2}]$ and $(\mathrm{Re}[t_0^{D_1}] + \mathrm{Re}[t_0^{D_2}])/2 = 1/4T_1 + nT_1$, where n is an integral, and $\mathrm{Re}[t_0]$ and $\mathrm{Im}[t_0]$ represent the real and imaginary parts of the ionization time of the direct electron, respectively. With this in mind, we omit the superscript of $\mathrm{Im}[t_0]$ in the following, and the interference shift $\delta\theta$ in

Eq. (10) is written as

$$
\delta\theta = \frac{2p_x F_2 \sin\varphi}{\omega_2^2} \sin\left(\omega_2 \mathrm{Re}\left[t_0^{D_1}\right]\right) \cosh(\omega_2 \mathrm{Im}[t_0])
$$
$$
+ \frac{-F_1 F_2 \sin\varphi}{3\omega_1^2 \omega_2}\Big[\cos\left(3\omega_1 \mathrm{Re}\left[t_0^{D_1}\right]\right) \cosh(3\omega_1 \mathrm{Im}[t_0])
$$
$$
- 3\cos\left(\omega_1 \mathrm{Re}\left[t_0^{D_1}\right]\right) \cosh(\omega_1 \mathrm{Im}[t_0])\Big]
$$
$$
+ U_p^{\mathrm{SH}}\left(2\mathrm{Re}\left[t_0^{D_1}\right] - \frac{T_1}{2}\right) - \frac{U_p^{\mathrm{SH}} \cos 2\varphi}{\omega_2}
$$
$$
\times \sin\left(2\omega_2 \mathrm{Re}\left[t_0^{D_1}\right]\right) \cosh(2\omega_2 \mathrm{Im}[t_0]). \quad (11)
$$

Here, $U_p^{\mathrm{SH}} = F_2^2/4\omega_2^2$ denotes the ponderomotive energy of the SH field. In Eq. (11), U_p^{SH} is a higher-order small term, and it can be approximately dropped. Thus, $\delta\theta$ of Eq. (11) is further simplified as

$$
\delta\theta = \frac{2p_x F_2 \sin\varphi}{\omega_2^2} \sin\left(\omega_2 \mathrm{Re}\left[t_0^{D_1}\right]\right) \cosh(\omega_2 \mathrm{Im}[t_0])
$$
$$
+ \frac{-F_1 F_2 \sin\varphi}{3\omega_1^2 \omega_2}\Big[\cos\left(3\omega_1 \mathrm{Re}\left[t_0^{D_1}\right]\right) \cosh(3\omega_1 \mathrm{Im}[t_0])
$$
$$
- 3\cos\left(\omega_1 \mathrm{Re}\left[t_0^{D_1}\right]\right) \cosh(\omega_1 \mathrm{Im}[t_0])\Big]. \quad (12)
$$

This shows that the quantity $\delta\theta$ maximizes at $\varphi = 0.5\pi$, and the maximum of $\delta\theta$ sensitively depends on p_x through the complex ionization time of direct electron. Equation (12) describes the origination of the temporal double-slit interference shift.

The periodic oscillation of $\delta\theta$ for different p_x in Figs. 4(e) and 4(f) suggests we fit the relative phase dependence with the trigonometric function $\delta\theta = \delta\theta_m \cos(\varphi - \varphi_m)$, where the quantity $\delta\theta_m$ denotes the amplitude of the oscillation and φ_m shows the phase where $\delta\theta$ maximizes. Technically, the two quantities can be determined by Fourier transforming $\delta\theta$ with respect to φ for each p_x [64,65]. The obtained $\delta\theta_m$ is displayed in Fig. 5(a), which enables us to resolve the temporal information of electron. For comparison, the predictions of the QO model, the QO model with artificially setting $\mathrm{Im}[t_0] = 0$, and the classical model [with $I_p = 0$ in the saddle-point equation of Eqs. (9)] are also displayed in Fig. 5(a). It is shown that for the cut of $p_y = 0$, the data from the classical model and the QO model with artificially setting $\mathrm{Im}[t_0] = 0$ agree well with each other but deviate seriously from the TDSE data. For the QO model, the predicted $\delta\theta_m$ shows an excellent agreement with the TDSE result. It means that the quantity $\delta\theta_m$ is very sensitive to the imaginary part of the ionization time. For the cut of $p_y = 0.2$ a.u., the predicted results are almost similar to that of the cut at $p_y = 0$.

With Eq. (12), we reconstruct the imaginary part of the ionization time of direct electron. Note that in our reconstruction, we only focused on the imaginary part of the ionization time. Previous studies have confirmed that the real part of the ionization time agrees well with the prediction of the QO model [66]. In our reconstruction, we have assumed that the real part of ionization time equals the data from QO model. The reconstructions are demonstrated in Fig. 5(b), where $\mathrm{Im}[t_0]$ as a function of p_x. Clearly, the result for $p_x \in [-1.4, -0.8]$ a.u agrees well with the QO model result. In the QO model, the
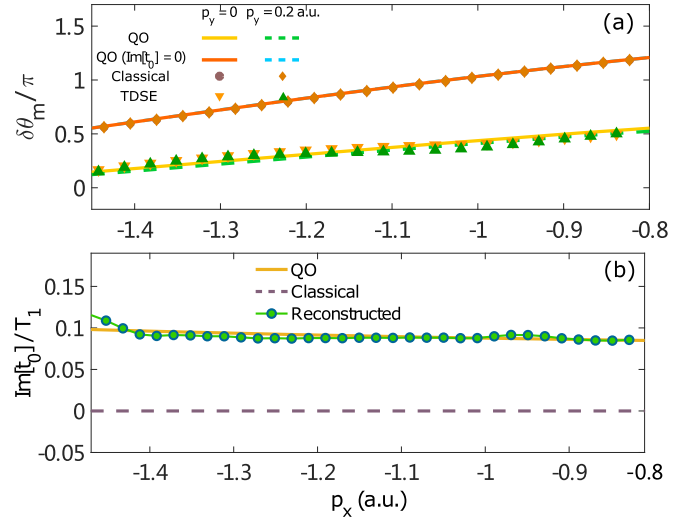
FIG. 5. (a) $\delta\theta_m$ extracted from the TDSE results (upside-down triangles and regular triangles) and predicted by the QO model (solid yellow line and dashed green line), QO model with $\mathrm{Im}[t_0] = 0$ (solid red line and dashed blue line) and classical model (dots and diamonds) for the cuts of $p_y = 0$ and $p_y = 0.2$ a.u., respectively. (b) Imaginary part of ionization time reconstructed from the TDSE data (dotted green line) and calculated by the QO model (solid yellow line) and classical model (dashed purple line), respectively.

ionization time is a complex number and its imaginary part relates to the inverse ionization rate and is interpreted as the time needed for electron passing through the tunneling barrier. In previous studies about tunneling ionization process, a zero or Keldysh time for the imaginary part of the ionization time was assumed [19,67]. In our case, there is no such assumption. We mention that the imaginary time from the QO model is consistent with the Keldysh time which was first introduced by Keldysh [15,29,68,69] and it characterizes the tunneling of the electron through a barrier formed by the atomic potential and the instantaneous electric field of the laser field. Recently, it has been reported that the imaginary time is crucial important for the electron attosecond dynamics of strong-field ionization and it closely associates to the predicted ultrafast phenomena [70,71]. Accurately retrieving this time is vital for thorough understanding of the strong-field processes and for further performing their applications. In our scheme, the imaginary ionization time for the direct electron is accurately retrieved.

IV. CONCLUSION

In summary, with a temporal double-slit interferometer, we retrieved the time information of the direct electron in strong-field tunneling ionization. This was a complementary to previous studies, where the temporal properties for the tunneling process of the rescattering electron were reconstructed based on the recollision-induced phenomena. In our scheme, we added a weak perturbative SH to the FM driving field and monitored the shift of the temporal double-slit interference. The key point was that the complicated Coulomb interaction did not affect the interference shift and can be safely canceled. Our results showed that the response of the temporal double-slit fringes to the perturbation was very sensitive to the imaginary part of the complex ionization time of the direct

electron. By analyzing the interference shift, the imaginary ionization time was reconstructed. The reconstruction agreed well with the time obtained from the QO model. This work provides a general tool to resolve the strong-field tunneling ionization in atoms and molecules, and it will encourage one applying the subcycle interferometer to investigate ultrafast dynamics in more complex molecules.

[1] G. G. Paulus, W. Nicklich, H. Xu, P. Lambropoulos, and H. Walther, Plateau in Above Threshold Ionization Spectra, Phys. Rev. Lett. **72**, 2851 (1994).

[2] W. Becker, F. Grasbon, R. Kopold, D. B. Milošević, G. G. Paulus, and H. Walther, Above-threshold ionization: From classical features to quantum effect, Adv. At. Mol. Opt. Phys. **48**, 35 (2002).

[3] M. Ferray, A. L'Huillier, X. F. Li, L. A. Lompré, G. Mainfray, and C. Manus, Multiple-harmonic conversion of 1064 nm radiation in rare gases, J. Phys. B **21**, L31 (1988).

[4] J. Li, Q. Zhang, L. Li, X. Zhu, T. Huang, P. Lan, and P. Lu, Orientation dependence of high-order harmonic generation in nanowire, Phys. Rev. A **99**, 033421 (2019).

[5] B. Wang, L. He, Y. He, Y. Zhang, R. Shao, P. Lan, and Q. Zhang, Characterizing the ellipticity of an isolated attosecond pulse, Opt. Express **27**, 30172 (2019).

[6] Z. Yang, W. Cao, X. Chen, J. Zhang, Y. Mo, H. Xu, K. Mi, Q. Zhang, P. Lan, and P. Lu, All-optical frequency resolved optical gating for isolated attosecond pulse reconstruction, arXiv:1911.06427.

[7] B. Walker, B. Sheehy, L. F. DiMauro, P. Agostini, K. J. Schafer, and K. C. Kulander, Precision Measurement of Strong Field Double Ionization of Helium, Phys. Rev. Lett. **73**, 1227 (1994).

[8] W. Becker, X. J. Liu, P. J. Ho, and J. H. Eberly, Theories of photoelectron correlation in laser-driven multiple atomic ionization, Rev. Mod. Phys. **84**, 1011 (2012).

[9] Y. Zhou, C. Huang, Q. Liao, and P. Lu, Classical Simulations Including Electron Correlations for Sequential Double Ionization, Phys. Rev. Lett. **109**, 053004 (2012).

[10] Y. Zhao, Y. Zhou, J. Liang, Z. Zeng, Q. Ke, Y. Liu, M. Li, and P. Lu, Frustrated tunneling ionization in the elliptically polarized strong laser field, Opt. Express **27**, 21689 (2019).

[11] A. Tong, Q. Li, X. Ma, Y. Zhou, and P. Lu, Internal collision induced strong-field nonsequential double ionization in molecules, Opt. Express **27**, 6415 (2019).

[12] X. Huang, Q. Zhang, S. Xu, X. Fu, X. Han, W. Cao, and P. Lu, Coulomb focusing in retrapped ionization with near-circularly polarized laser field, arXiv:1911.09805.

[13] F. Krausz and M. Ivanov, Attosecond physics, Rev. Mod. Phys. **81**, 163 (2009).

[14] L. Peng, W. Jiang, J. Geng, W. Xiong, and Q. Gong, Tracing and controlling electronic dynamics in atoms and molecules by attosecond pulses, Phys. Rep. **575**, 1 (2015).

[15] L. V. Keldysh, Ionization in the field of a strong electromagnetic wave, J. Exp. Theor. Phys. **20**, 1307 (1965).

[16] G. L. Yudin and M. Y. Ivanov, Nonadiabatic tunnel ionization: Looking inside a laser cycle, Phys. Rev. A **64**, 013409 (2001).

[17] W. Xie, M. Li, S. Luo, M. He, K. Liu, Q. Zhang, Y. Zhou, and P. Lu, Nonadiabaticity-induced ionization time shift in strong-field tunneling ionization, Phys. Rev. A **100**, 023414 (2019).

[18] S. Luo, M. Li, W. Xie, K. Liu, Y. Feng, B. Du, Y. Zhou, and P. Lu, Exit momentum and instantaneous ionization rate of nonadiabatic tunneling ionization in elliptically polarized laser fields, Phys. Rev. A **99**, 053422 (2019).

[19] D. Shafir, H. Soifer, B. D. Bruner, M. Dagan, Y. Mairesse, S. Patchkovskii, M. Y. Ivanov, O. Smirnova, and N. Dudovich, Resolving the time when an electron exits a tunneling barrier, Nature (London) **485**, 343 (2012).

[20] O. Pedatzur, G. Orenstein, V. Serbinenko, H. Soifer, B. D. Bruner, A. J. Uzan, D. S. Brambila, A. G. Harvey, L. Torlina, F. Morales, O. Smirniva, and N. Dudovich, Attosecond tunneling interferometry, Nat. Phys. **11**, 815 (2015).

[21] J. Tan, Y. Zhou, M. He, Y. Chen, Q. Ke, J. Liang, X. Zhu, M. Li, and P. Lu, Determination of the Ionization Time Using Attosecond Photoelectron Interferometry, Phys. Rev. Lett. **121**, 253203 (2018).

[22] J. Tan, Y. Zhou, M. He, Q. Ke, J. Liang, Y. Li, M. Li, and P. Lu, Time-resolving tunneling ionization via strong-field photoelectron holography, Phys. Rev. A **99**, 033402 (2019).

[23] M. Li, H. Xie, W. Cao, S. Luo, J. Tan, Y. Feng, B. Du, W. Zhang, Y. Li, Q. Zhang, P. Lan, Y. Zhou, and P. Lu, Photoelectron Holographic Interferometry to Probe the Longitudinal Momentum Offset at the Tunnel Exit, Phys. Rev. Lett. **122**, 183202 (2019).

[24] P. B. Corkum, Plasma Perspective on Strong Field Multiphoton Ionization, Phys. Rev. Lett. **71**, 1994 (1993).

[25] P. Salières, B. Carré, L. L. Déroff, F. Grasbon, G. G. Paulus, H. Walther, R. Kopold, W. Becker, D. B. Milošević, A. Sanpera, and M. Lewenstein, Feynman's path-integral approach for intense-laser-atom interactions, Science **292**, 902 (2001).

[26] P. Eckle, A. N. Pfeiffer, C. Cirelli, A. Staudte, R. Dörner, H. G. Muller, M. Büttiker, and U. Keller, Attosecond ionization and tunneling delay time measurements in helium, Science **322**, 1525 (2008).

[27] L. Torlina, F. Morales, J. Kaushal, I. Ivanov, A. Kheifets, A. Zielinski, A. Scrinzi, H. G. Muller, S. Sukiasyan, M. Ivanov, and O. Smirnova, Interpreting attoclock measurements of tunneling times, Nat. Phys. **11**, 503 (2015).

[28] N. Camus, E. Yakaboylu, L. Fechner, M. Klaiber, M. Laux, Y. Mi, K. Z. Hatsagortsyan, T. Pfeifer, C. H. Keitel, and R. Moshammer, Experimental Evidence for Quantum Tunneling Time, Phys. Rev. Lett. **119**, 023201 (2017).

[29] A. M. Perelomov, V. S. Popov, and M. V. Terent'ev, Ionization of atoms in an alternating electric field: II, J. Exp. Theor. Phys. **24**, 207 (1967).

[30] M. Ivanov, M. Spanner, and O. Smirnova, Anatomy of strong field ionization, J. Mod. Opt. **52**, 165 (2005).

[31] Y. Huismans, A. Rouzée, A. Gijsbertsen, J. Jungmann, A. Smolkowska, P. Logman, F. Lépine, C. Cauchy, S. Zamith, T. Marchenko, J. Bakker, G. Berden, B. Redlich, A. van der Meer, H. Muller, W. Vermin, K. Schafer, M. Spanner, M. Ivanov, O. Smirnova, D. Bauer, S. Popruzhenko, and M. Vrakking, Time-resolved holography with photoelectrons, Science **331**, 61 (2011).

[32] Y. Huismans, A. Gijsbertsen, A. S. Smolkowska, J. H. Jungmann, A. Rouzée, P. S. W. M. Logman, F. Lépine, C. Cauchy, S. Zamith, T. Marchenko, J. M. Bakker, G. Berden, B. Redlich, A. F. G. van der Meer, M. Yu. Ivanov, T.-M. Yan, D. Bauer, O. Smirnova, and M. J. J. Vrakking, Scaling Laws for Photoelectron Holography in the Midinfrared Wavelength Regime, Phys. Rev. Lett. **109**, 013002 (2012).

[33] F. Lindner, M. G. Schätzel, H. Walther, A. Baltuška, E. Goulielmakis, F. Krausz, D. B. Milošević, D. Bauer, W. Becker, and G. G. Paulus, Attosecond Double-Slit Experiment, Phys. Rev. Lett. **95**, 040401 (2005).

[34] D. Arbó, E. Persson, and J. Burgdörfer, Time double-slit interferences in strong-field tunneling ionization, Phys. Rev. A **74**, 063407 (2006).

[35] D. Arbó, K. L. Ishikawa, K. Schiessl. E. Persson, and J. Burgdörfer, Intracycle and intercycle interferences in above-threshold ionization: The time grating, Phys. Rev. A **81**, 021403(R) (2010).

[36] D. Arbó, K. L. Ishikawa, K. Schiessl. E. Persson, and J. Burgdörfer, Diffraction at a time grating in above-threshold ionization: The influence of the Coulomb potential, Phys. Rev. A **82**, 043426 (2010).

[37] D. Arbó, K. L. Ishikawa, E. Persson, and J. Burgdörfer, Doubly differential diffraction at a time grating in above-threshold ionization: Intracycle and intercycle interferences, Nucl. Instrum. Methods B **279**, 24 (2012).

[38] P. A. Korneev, S. V. Popruzhenko, S. P. Goreslavski, T.-M. Yan, D. Bauer, W. Becker, M. Kübel, M. F. Kling, C. Rödel, M. Wünsche, and G. G. Paulus, Interference Carpets in Above-Threshold Ionization: From the Coulomb-Free to the Coulomb-Dominated Regime, Phys. Rev. Lett. **108**, 223601 (2012).

[39] T.-M. Yan and D. Bauer, Sub-barrier Coulomb effects on the interference pattern in tunneling-ionization photoelectron spectra, Phys. Rev. A **86**, 053403 (2012).

[40] D. Arbó, S. Nagele, X.-M. Tong, X. Xie, M. Kitzler, and J. Burgdörfer, Interference of electron wave packets in atomic ionization by subcycle sculpted laser pulses, Phys. Rev. A **89**, 043414 (2014).

[41] X. Xie, S. Roither, D. Kartashov, E. Persson, D. G. Arbó, L. Zhang. S. Gräfe, M. S. Schöffler, J. Burgdörfer, A. Baltuška, and M. Kitzler, Attosecond Probe of Valence-Electron Wave Packets by Subcycle Sculpted Laser Fields, Phys. Rev. Lett. **108**, 193004 (2012).

[42] X. Xie, S. Roither, S. Gräfe, D. Kartashov, E. Persson, C. Lemell, L. Zhang, M. S. Schöffler, A. Baltuška, J. Burgdörfer, and M. Kitzler, Probing the influence of the Coulomb field on atomic ionization by sculpted two-color laser fields, New J. Phys. **15**, 043050 (2013).

[43] M. Richter, M. Kunitski, M. Schöffler, T. Jahnke, L. P. H. Schmidt, M. Li, Y. Liu, and R. Dörner, Streaking Temporal Double-Slit Interference by an Orthogonal Two-Color Laser Field, Phys. Rev. Lett. **114**, 143001 (2015).

[44] M. Li, J. Geng, M. Liu, X. Zheng, L. Peng, Q. Gong, and Y. Liu, Spatial-temporal control of interferences of multiple tunneling photoelectron wave packets, Phys. Rev. A **92**, 013416 (2015).

[45] M. Protopapas, C. H. Keitel, and P. L. Knight, Atomic physics with super-high intensity lasers, Rep. Prog. Phys. **60**, 389 (1997).

[46] M. D. Feit, J. A. Fleck, and A. Steiger, Solution of the Schrödinger equation by a spectral method, J. Comput. Phys. **47**, 412 (1982).

[47] X. Tong, K. Hino, and N. Toshima, Phase-dependent atomic ionization in few-cycle intense laser fields, Phys. Rev. A **74**, 031405 (2006).

[48] P. He, N. Takemoto, and F. He, Photoelectron momentum distribution of atomic and molecular systems in strong circularly or elliptically polarized laser field, Phys. Rev. A **91**, 063413 (2015).

[49] M. He, Y. Li, Y. Zhou, M. Li, and P. Lu, Temporal and spatial manipulation of the recolliding wave packet in strong-field photoelectron holography, Phys. Rev. A **93**, 033406 (2016).

[50] D. B. Milošević and W. Becker, Role of long quantum orbits in high-order harmonic generation, Phys. Rev. A **66**, 063417 (2002).

[51] D. B. Milošević, G. G. Paulus, D. Bauer, and W. Becker, Above-threshold ionization by few-cycle pulses, J. Phys. B **39**, R203 (2006).

[52] P. Agostini, F. Fabre, G. Mainfray, G. Petite, and N. K. Rahman, Free-Free Transitions Following Six-Photon Ionization of Xenon Atoms, Phys. Rev. Lett. **42**, 1127 (1979).

[53] Y. Feng, M. Li, S. Luo, K. Liu, B. Du, Y. Zhou, and P. Lu, Semiclassical analysis of photoelectron interference in a synthesized two-color laser pulse, Phys. Rev. A **100**, 063411 (2019).

[54] X. Bian and A. D. Bandrauk, Attosecond Time-Resolved Imaging of Molecular Structure by Photoelectron Holography, Phys. Rev. Lett. **108**, 263003 (2012).

[55] M. Meckel, A. Staudte, S. Patchkovskii, D. M. Villeneuve, P. B. Corkum, R. Dörner, and M. Spanner, Signatures of the continuum electron phase in molecular strong-field photoelectron holography, Nat. Phys. **10**, 594 (2014).

[56] Y. Zhou, O. I. Tolstikhin, and T. Morishita, Near-Forward Rescattering Photoelectron Holography in Strong-Field Ionization: Extraction of the Phase of the Scattering Amplitude, Phys. Rev. Lett. **116**, 173001 (2016).

[57] W. Yang, H. Zhang, C. Lin, J. Xu, Z. Sheng, X. Song, S. Hu, and J. Chen, Momentum mapping of continuum-electron wave-packet interference, Phys. Rev. A **94**, 043419 (2016).

[58] S. G. Walt, N. B. Ram, M. Atala, N. I. S. Shilovski, A. Conta, D. Baykusheva, M. Lein, and H. J. Wörner, Dynamics of valence-shell electrons and nuclei probed by strong-field holography and rescattering, Nat. Commun. **8**, 15651 (2017).

[59] M. He, Y. Li, Y. Zhou, M. Li, W. Cao, and P. Lu, Direct Visualization of Valence Electron Motion Using Strong-Field Photoelectron Holography, Phys. Rev. Lett. **120**, 133204 (2018).

[60] Y. Liu, J. Tan, M. He, H. Xie, Y. Qin, Y. Zhao, M. Li, Y. Zhou, and P. Lu, Photoelectron holographic interferences from multiple returning in strong-field tunneling ionization, Opt. Quant. Electron. **51**, 145 (2019).

[61] Q. Ke, Y. Zhou, J. Tan, M. He, J. Liang, Y. Zhao, M. Li, and P. Lu, Two-dimensional photoelectron holography in strong-field tunneling ionization by counter rotating two-color circularly polarized laser pulses, Opt. Express **27**, 32193 (2019).

[62] J. Liang, Y. Zhou, J. Tan, M. He, Q. Ke, Y. Zhao, M. Li, W. Jiang, and P. Lu, Low-energy photoelectron interference structure in attosecond streaking, Opt. Express **27**, 37975 (2019).

[63] M. Li, J. Yuan, X. Sun, J. Yu, Q. Gong, and Y. Liu, Recollision-induced subcycle interference of molecules in strong laser fields, Phys. Rev. A **89**, 033425 (2014).

[64] J. Tan, Y. Zhou, M. Li, M. He, Y. Liu, and P. Lu, Accurate measurement of laser intensity using photoelectron interference in strong-field tunneling ionization, Opt. Express **26**, 20063 (2018).

[65] J. Tan, Y. Li, Y. Zhou, M. He, Y. Chen, M. Li, and P. Lu, Identifying the contributions of multiple-returning recollision orbits in strong-field above-threshold ionization, Opt. Quant. Electron. **50**, 57 (2018).

[66] J. Henkel and M. Lein, Analysis of electron trajectories with two-color strong-field ionization, Phys. Rev. A **92**, 013422 (2015).

[67] J. Zhao and M. Lein, Determination of Ionization and Tunneling Times in High-Order Harmonic Generation, Phys. Rev. Lett. **111**, 043901 (2013).

[68] V. S. Popov, V. P. Kuznetsov, and A. M. Perelomov, Quansicalssical approximation for nonstationary problems, Sov. Phys. JETP **26**, 222 (1968).

[69] V. P. Kuznetsov, A. M. Perelomov, and V. S. Popov, Quansicalssical approximation in ionization problems, Sov. Phys. JETP **27**, 616 (1968).

[70] V. D. Mur, S. V. Popruzhenko, and V. S. Popov, Energy and momentum spectra of photoelectrons under conditions of ionization by strong laser radiation (the case of elliptic polarization), J. Exp. Theor. Phys. **92**, 777 (2001).

[71] M. Han, P. Ge, Y. Shao, M. Liu, Y. Deng, C. Wu, Q. Gong, and Y. Liu, Revealing the Sub-Barrier Phase Using a Spatiotemporal Interferometer with Orthogonal Two-Color Laser Fields of Comparable Intensity, Phys. Rev. Lett. **119**, 073201 (2017).